Three-Dimensional Configuration of Subretinal Fluid in Central Serous Chorioretinopathy

Soh-Eun Ahn,[1] Jaeryung Oh,[1] Jong-Hyun Oh,[2] In Kyung Oh,[3] Seong-Woo Kim,[1] and Kuhl Huh[1]

[1]Department of Ophthalmology, Korea University College of Medicine, Seoul, Korea
[2]Department of Ophthalmology, Dongguk University, Ilsan Hospital, Goyang, Korea
[3]Department of Ophthalmology, Wonkwang University, Sanbon Hospital, Seoul, Korea

Correspondence: Jaeryung Oh, Department of Ophthalmology, Korea University College of Medicine, 126-1 Anam-dong 5-ga, Sungbuk-gu, Seoul, 136-705, Korea; ojr4991@korea.ac.kr.

Submitted: April 23, 2013
Accepted: July 27, 2013

Citation: Ahn S-E, Oh J, Oh J-H, Oh IK, Kim S-W, Huh K. Three-dimensional configuration of subretinal fluid in central serous chorioretinopathy. *Invest Ophthalmol Vis Sci*. 2013;54:5944–5952. DOI:10.1167/iovs.13-12279

Purpose. The purpose of this study was to characterize the 3-dimensional (3D) configuration of subretinal fluid (SRF) in idiopathic central serous chorioretinopathy (CSC) using spectral-domain optical coherence tomography (SDOCT).

Methods. The OCT images of patients with CSC were reviewed retrospectively. The 3D configurations of SRF were assessed using a modified segmentation algorithm of SDOCT. The differences of the configurations between acute and chronic CSC were compared. For the patients with acute CSC, we investigated a possible relationship between early change in 3D configuration and disease prognosis.

Results. We included 69 eyes of 68 patients in this study. The mean volume, the greatest basal diameter (GBD), and the area of SRF were not different between acute and chronic CSC. The mean peak height (PH) of SRF and the ratio of PH to GBD in acute CSC (298.13 ± 92.67 μm, 9.44 ± 2.57%) were significantly greater than those in chronic CSC (192.97 ± 71.05 μm, 5.97 ± 1.90%; $P < 0.001$, $P < 0.001$, respectively). In patients with acute CSC, the early changing pattern of 3D configurations was significantly different according to the SRF prognosis ($P = 0.003$). In situ decrease of SRF was observed in 94.7% of the spontaneously resolving group. However, downward elongation of SRF was observed more frequently in the persistent group (58.3%) than in the spontaneously resolving group (6.3%).

Conclusions. The 3D configurations of SRF were different between acute and chronic CSC. In patients with acute onset, the early change of 3D configuration was different and varied according to the SRF prognosis.

Keywords: central serous chorioretinopathy, optical coherence tomography, three-dimensional configuration, subretinal fluid

Idiopathic central serous chorioretinopathy (CSC) is characterized by serous neurosensory retinal detachment in the macular area.[1] Increased permeability of the choriocapillaris leads to focal or diffuse dysfunction of the RPE, which causes detachment of the neurosensory retina.[2] In general, acute CSC resolves spontaneously, and the patient's visual acuity (VA) returns to normal. However, some patients have prolonged and recurrent retinal detachment, which may result in permanent poor vision. The prognosis of CSC is difficult to predict in clinical practice, because it has a broad spectrum of presentations and dynamic variations during its progress.

Introduction of optical coherence tomography (OCT) technology in the field of ophthalmology has initiated a new era for CSC researches.[3] Various morphologic features of CSC, including retinal detachment, fibrinous exudation, and cystic changes within the retina, have been reported.[4–13] Studies investigating the microstructures in CSC have provided more information on its pathophysiology.[14–19] In addition to the tomographic data, OCT provides three-dimensional (3D) information about macular configuration.[20] This modality can generate rendered volumetric views of retinal structure similar to magnetic resonance images. OCT-based measurements, such as macular volume and Early Treatment Diabetic Retinopathy Study (ETDRS) grid retinal thickness, have proven to be useful for estimating the volume of clinically relevant features in macular diseases. Various studies have measured the volume of subretinal fluid (SRF) using OCT.[21–23] Nakajima et al. used this method to determine the volume of SRF by multiplying the size of the area of the retinal detachment by the mean height of the retinal detachment.[22] Heussen et al. suggested a simplified technique to measure the volume.[23] However, 3D configuration of SRF has not been investigated widely in CSC.

Recent developments in spectral-domain OCT (SDOCT) technology have provided an advanced built-in program for segmentation of the retinal layers. Furthermore, it is possible to modify the segmentation line, which has been set-up automatically, and then calibrate the segmentation errors.[24] This technology makes it possible to reconstruct the 3D image of SRF, and to estimate the extent and change of SRF (Fig. 1). In this study, using the modified segmentation algorithms of SDOCT, we investigated the 3D characteristics of SRF and their relationship to the disease prognosis.

Methods

The study protocol was approved by the Institutional Review Board at Korea University. This study followed the tenets of the Declaration of Helsinki.

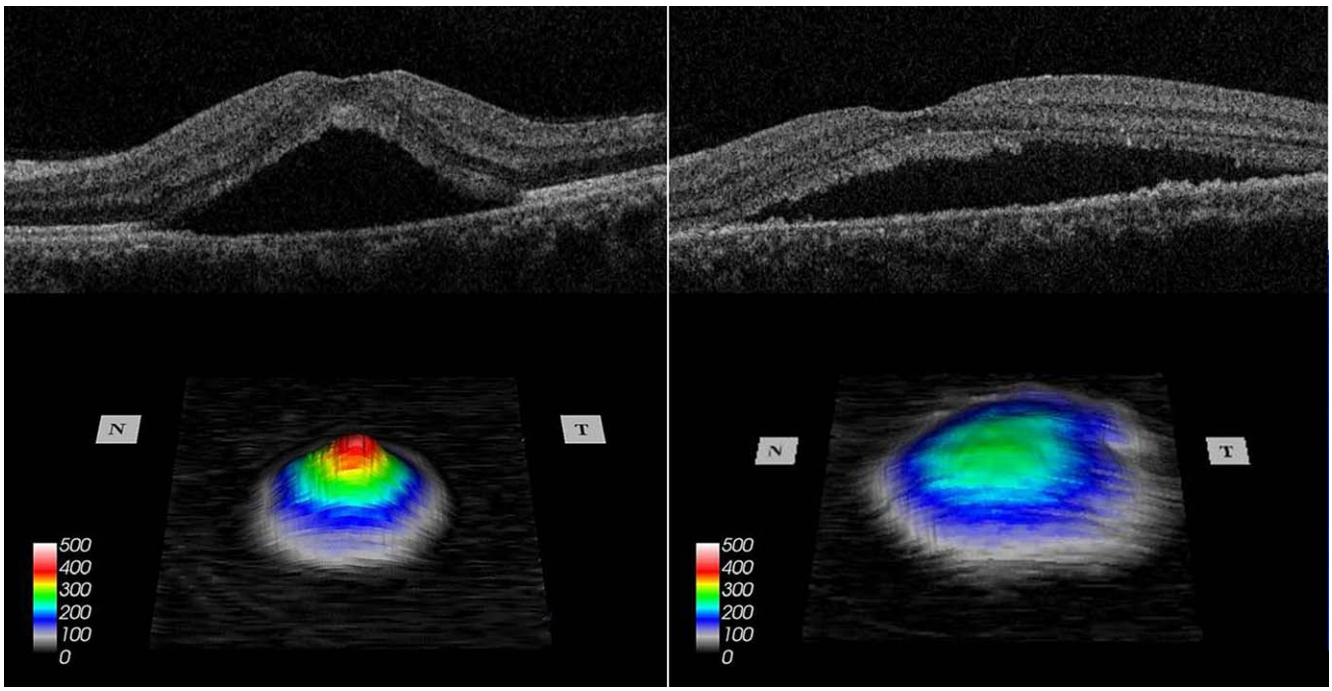

FIGURE 1. 3D images of SRF in acute (*bottom left*) and chronic (*bottom right*) CSC.

Data Collection

The medical records of patients with idiopathic CSC who had been examined at Korea University Medical Center between July 2009 and November 2012 were reviewed retrospectively. All patients included in the study had undergone a complete ophthalmic examination, including fluorescence angiography (FA) and SDOCT at their initial visit, and had received consecutive follow-up SDOCT examinations.

Idiopathic CSC was diagnosed based on the presence of serous detachment of neurosensory retina involving the macula, which was confirmed by SDOCT, and leakage at the level of RPE on FA. The patients were classified into two groups according to symptom duration before the initial visit, which was adopted from the classification system suggested in previous studies.[25–27] Patients were diagnosed with acute CSC when they demonstrated an onset of symptoms, such as visual loss, metamorphopsia, chromatopsia, or micropsia within the three months before initial OCT examination. Patients were classified with chronic CSC when they presented with symptom onset that had occurred more than three months before the initial visit.

This study excluded any eyes with other retinal abnormalities, such as choroidal neovascularization, retinal vascular disease, or intraocular inflammation (Supplementary Table S1). In addition, eyes with a history of previous treatment, including macular photocoagulation, photodynamic therapy, or intravitreal antivascular endothelial growth factor injection, also were excluded. Finally, patients who had steroid-induced CSC or organ transplant–associated CSC also were excluded. This study analyzed only SDOCT images that had an image quality factor greater than 45.

Measurement of 3D Configuration

The SDOCT (3D OCT-1000 Mark II, software version 3.20; Topcon Corp., Tokyo, Japan) used in this study had a wavelength of 840 nm, a horizontal resolution of $\leq$20 μm, and an axial resolution of up to 5 μm. The imaging speed was 27,000 axial scans per second. Patients underwent SDOCT evaluation using 3D scanning protocols with 128 B-scans (512 A-scans per B-scan) of a 6×6 mm area. This device contains a camera for obtaining color images of the fundus just after the OCT images are taken. From the 3D volume scan images, the automatically measured data of the central subfield thickness, the central point thickness, and the total macular volume were obtained.

Three-D configurations of SRF or pigment epithelial detachment (PED) were characterized with modified OCT parameters as follows: volume; peak height (PH), greatest basal diameter (GBD), and the basal area; and ratio of PH to GBD (PH/GBD). In addition, only for SRF, vertical eccentricity and type of basal area were identified as indicators of gravity effect on SRF configuration. SRF volume was estimated using a built-in segmentation-modifying tool of SDOCT (Fig. 2).[24] A similar process was performed to calculate the volume of PED. Pure retina layer (PRL) volume was defined as that of the macula area which excluded SRF and was calculated by subtracting the volume of SRF from the total macular volume. The perpendicular height of SRF was measured from the RPE line to the outer segment tips of the photoreceptors. For PED, the height was measured from the line of Bruch's membrane to the RPE line, both using a built-in caliper function. PH was defined as the greatest height of SRF or PED. GBD and area of SRF were obtained from the segmentation map of the photoreceptor inner and outer segments (IS/OS) junction provided at the 3D volume scan, and in the case of PED, from the segmentation map of RPE (Fig. 3). After processing the IS/OS image or RPE segmentation map with the ImageJ software program (http://rsb.info.nih.gov/; National Institutes of Health, Bethesda, MD) the GBD and area of the lesions were measured. The ratio of PH to GBD was calculated by dividing the greatest height by the maximum lesion diameter, and was documented as a fraction of 100. Topographic locations of the PH and the center of SRF were documented as B-scan numbers, which corresponded to the volume scan (Fig. 4).

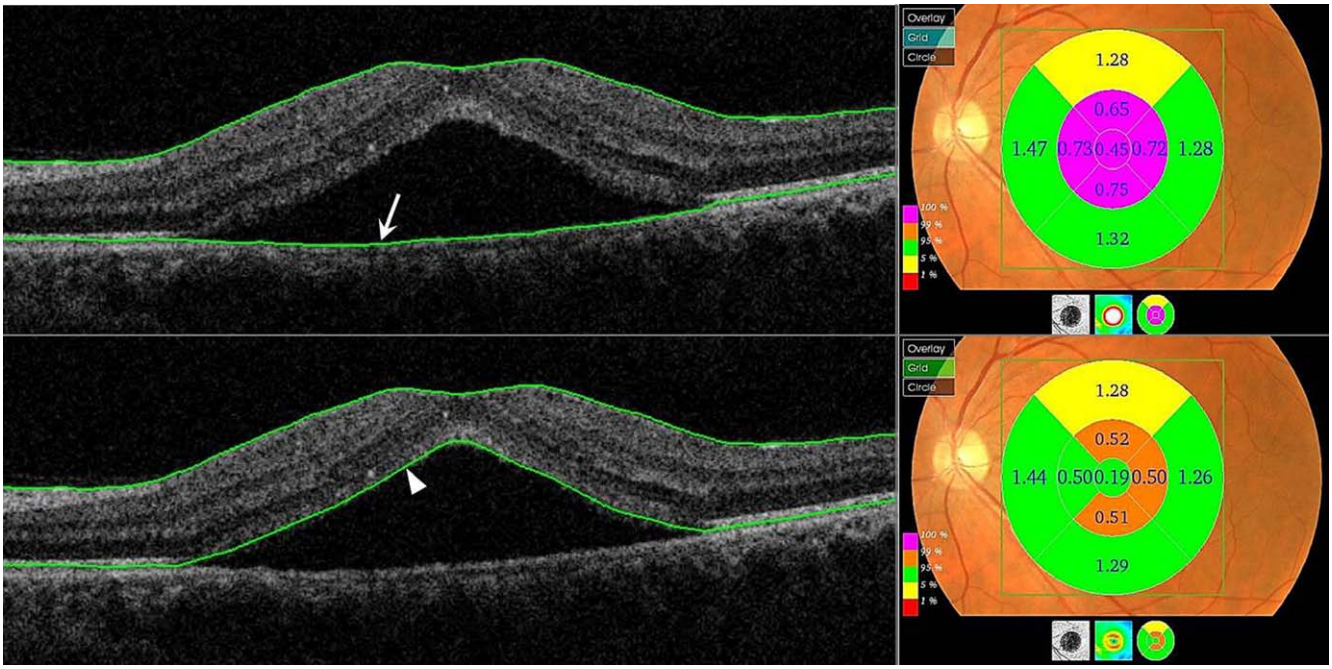

Figure 2. SRF volume estimation using a built-in segmentation-modifying tool of SDOCT. Segmentation lines for internal limiting membrane and RPE (*arrow*) were determined automatically for each of the volume scans, and the total macular volume was provided (*top right*). Using the modifying tool, the cursor line on the RPE was moved to the tips of the outer segments of the photoreceptors (*arrowhead*, *bottom*). We set the segmentation to follow the contour of the photoreceptor IS/OS layer when there was hyperreflective material hanging from the PRL into the SRF space. With this movement, the modified macular volume was determined excluding SRF (*bottom right*). The SRF volume was calculated by subtracting this modified macular volume from the total macular volume. Modified macular volume was regarded as the same as the pure retinal layer volume in this study.

Vertical eccentricity of SRF was identified as the percentage of vertical deviation of the PH point from the center of total lesions. The SRF basal area figures were categorized into two types according to the angle of GBD to the horizontal line. Circular or horizontal oval type was defined when the angle was less than 45°. Vertical oval type was defined when it was greater than 45°. The study compared the initial OCT parameters in relation to the 3D configurations between acute and chronic CSC.

3D Configuration Changes in Acute and Chronic CSC

The study investigated how the 3D configurations of SRF and PED changed during the early diagnostic period. The

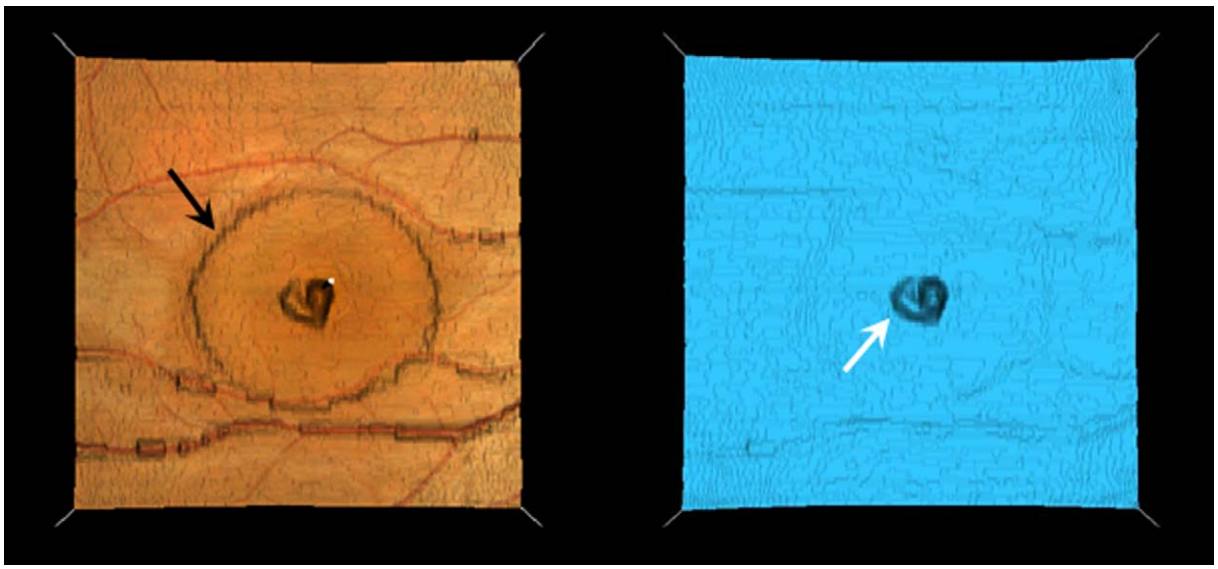

Figure 3. GBD and the basal area of SRF (*black arrow*) were measured in the segmentation map (*left*) generated at the reference plane of photoreceptor IS/OS junction. The parameters of PED (*white arrow*) was measured in the retinal pigment epithelium segmentation map (*right*).

Investigative Ophthalmology & Visual Science

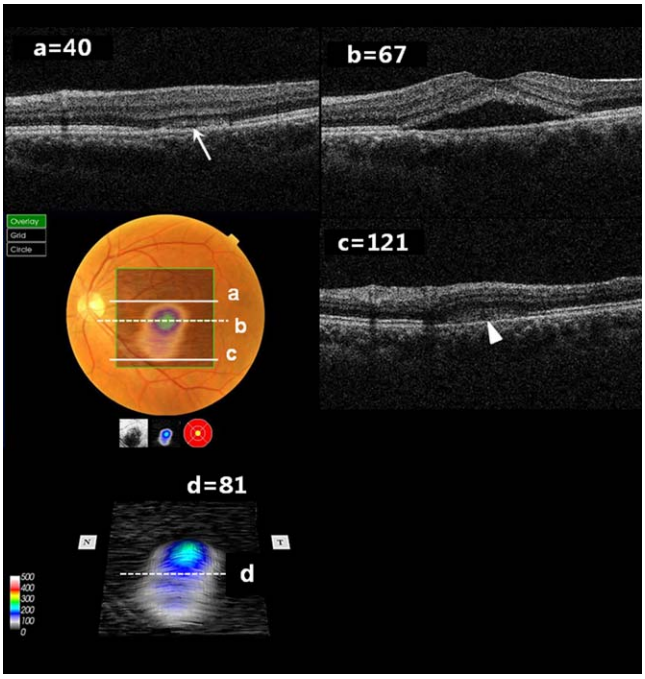

FIGURE 4. Vertical eccentricity. The scan numbers of the B-scan with an upper margin of SRF (**a**) and with a lower margin of SRF (**c**) were obtained. The interval between (**a**) and (**c**) was assumed to represent the vertical extent of the SRF lesion. The scan number of the B-scan with the point of SRF peak height (**b**) was determined by built-in software that used SDOCT. The center of SRF (**d**) was calculated as $(a+c)/2$. The percentage of vertical deviation between the peak height point and the center of SRF was assumed to represent the vertical eccentricity and was calculated as $(|b-d|/[c-a]) \times 100$ and given as a percentage (%).

changes of the OCT parameters between the initial and one month follow-up examinations were identified. We compared the change of OCT parameters during initial follow-up period between acute and chronic CSC. The changing pattern of SRF was evaluated using the "Compare" and "Overlay" functions in the OCT viewer program. It was classified into two types; in situ decrease type or downward elongated type (Fig. 5).

3D Configuration and Disease Prognosis in Acute CSC

Only for the patients with acute CSC, we investigated the relationship between the changing pattern of 3D configurations during initial period and the prognosis of SRF. The patients with acute CSC were categorized into two subgroups: the spontaneously resolving group, in which the SRF resolved completely within three months from the initial visit, and the persistent group, in which the SRF continued over three months of follow-up. Various OCT parameters related to 3D configuration were compared in the two subgroups.

Statistical Analysis

All data were analyzed using SPSS software version 20.0 (SPSS, Inc., Chicago, IL). A P value less than 0.05 was considered to be statistically significant. Results were expressed as mean ± SD. Significant differences in continuous variables, such as patient age, symptom duration, and variable OCT parameters, were identified using a t-test or a Mann-Whitney U test. Significant differences in categorical variables, such as sex, laterality of the affected eye, and type of basal area, were determined using a χ^2 test or Fisher's exact test. The change of SRF volume was correlated with other OCT parameters using Spearman's correlation analysis.

RESULTS

Patient Characteristics

After reviewing the records of 120 patients who were diagnosed with CSC at their initial visit, 69 eyes of 68 patients were selected for this study (Supplementary Fig. S1). Of the 69 eyes included in this study, 39 eyes had acute CSC and 30 eyes had chronic CSC. The mean age of the patients was 45.48 ± 7.48 years, and there was no statistically significant difference between the groups (Table 1). Of the patients 51 were male and 18 were female. At their initial visit, the mean symptom duration was 25 ± 24 days for acute CSC and 497 ± 632 days for chronic CSC. There were 25 recurrent cases, and there was no difference between the two groups ($P = 0.282$). All patients underwent FA examinations, except the three patients with allergies to fluorescein dye. The leakage patterns were classified into three types: inkblot (45.5%), smokestack (19.7%), and diffuse or mottled pattern (34.8%).

Characteristics of 3D Configuration

The mean central subfield thickness and the total macular volume were significantly greater in acute than chronic CSC ($P = 0.010$, 0.019, respectively, Table 2). The mean volume of PRL was greater in the acute CSC group compared to the chronic group ($P = 0.012$). However, there was no significant difference in the SRF volume. The detailed analysis of OCT parameters of SRF configurations indicated that the mean PH of SRF was greater in acute than in chronic CSC ($P < 0.001$). However, the mean GBD and the basal area were not different. The ratio of PH to GBD was 5.97 ± 1.90% in chronic CSC and was significantly lower than the 9.44 ± 2.57% value of the acute group ($P < 0.001$). Vertical eccentricity of SRF was greater in chronic CSC (15.80 ± 13.66%) than in acute CSC (7.10 ± 5.02%, $P = 0.002$). Vertical oval type was larger in percentage than circular or horizontal oval type in chronic CSC. However, that was not the case in acute CSC. PED was observed in 65 of the total 69 eyes (94.2%). The mean PH and the PH-to-GBD ratio of PED were significantly different between the two groups ($P = 0.010$, 0.008, respectively), but the volume, GBD, and area of PED were not significantly different.

3D Configuration Changes in Acute and Chronic CSC

Of the 69 eyes of 68 patients, 52 eyes of 51 patients underwent follow-up examination at one month and were included in this analysis (Table 3). A total of 31 eyes had acute CSC and 21 eyes had chronic CSC. The change of SRF volume was greater in the acute CSC than the chronic group ($P = 0.004$).The mean change of PH, GBD, and area of SRF were higher in acute CSC than in the chronic group ($P < 0.001$, $P = 0.004$, $P = 0.008$, respectively). The mean changes of OCT parameters of PED configurations were significantly different in volume, PH, and ratio of PH to GBD, but not for GBD or the basal area when the two groups were compared. In acute CSC, the change of SRF volume was

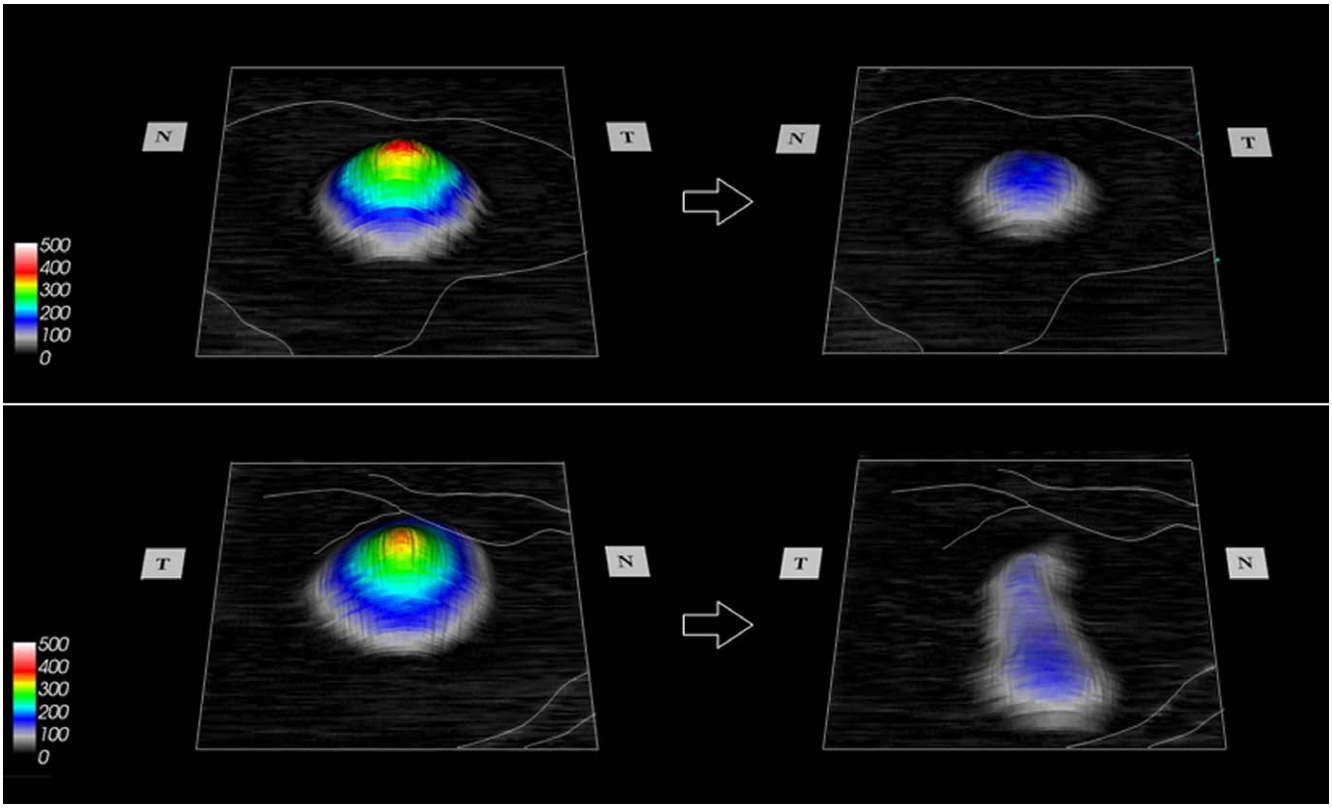

Figure 5. The 3D configuration of SRF at baseline (*left*) and follow-up examination after one month (*right*). The changing pattern of SRF was classified into two types; in situ decrease type (*top*) or downward elongated type (*bottom*).

correlated with those of PRL volume (*rho* = 0.363, *P* = 0.045). However, it was significant in chronic CSC (Table 4).

3D Configuration and Disease Prognosis in Acute CSC

Of the 31 patients with acute CSC, 29 patients received follow-up examinations until three months after the initial visit and were all included in this analysis. There were 17 patients placed in the spontaneously resolving group and 12 were placed in the persistent group (Table 5, Supplementary Table S1). The OCT parameters at the initial visit did not show significant differences between the two subgroups. However, the extent of change in OCT parameters was significantly greater in the spontaneously resolving group than in the persistent group. The SRF volume decreased during the first month at a rate of 77% in the spontaneously resolving group. This decreasing rate was greater than that of 27% in the persistent group. The changing pattern of SRF was significantly different between the two subgroups (*P* = 0.003). The percentage of eyes with in situ decrease type was larger in the spontaneously resolving group (94.7%) than in the persistent group (41.7%). The persistent group (58.3%) showed more frequent downward elongated type than the spontaneously resolving group (6.3%).

Discussion

In our study, we measured quantitatively the 3D configurations of SRF in CSC. The volume, basal area, or GBD of SRF were not different between acute and chronic CSC. PH of SRF was higher in the acute CSC than the chronic group; however, the actual measurement value could be subject to the total amount of SRF. Therefore, in the current study, we measured the ratio of PH to GBD (PH/GBD). The mean PH/GBD ratio was greater in acute than in chronic CSC. Because the amount of SRF varies in a clinical setting, the PH/GBD ratio might be a useful

Table 1. Patient Characteristics

	Acute CSC, *n* = 39	Chronic CSC, *n* = 30	*P* Value	Total, *n* = 69
Age, y	44.31 ± 7.46	47.00 ± 7.35	0.139*	45.48 ± 7.48
Sex, M:F	29:10	22:8	0.923†	51:18
Eye affected, OD:OS	17:22	13:17	0.983†	30:39
Symptom duration, d	25 ± 24	497 ± 632	<0.001*	230 ± 476
Recurrence history, first:recurrent	27:12	17:13	0.282†	44:25
FA finding, a:b:c	24:11:2, *n* = 37	6:2:21, *n* = 29	<0.001†	30:13:23, *n* = 66

FA finding indications: a, inkblot; b, smokestack; c, diffuse or mottled leakage.
* *t*-test for continuous variables.
† χ^2 for categorical variables. Continuous variables are expressed as mean ± SD.

Table 2. Three-Dimensional Configurations of CSC Using SDOCT at the Initial Visit

	Acute CSC, $n = 39$	Chronic CSC, $n = 30$	*P* Value*
CMT, μm	307.19 ± 35.59	287.13 ± 23.72	0.010
CPT, μm	437.23 ± 91.98	315.37 ± 96.46	<0.001
MV, mm^3	8.68 ± 0.99	8.18 ± 0.62	0.019
PRL volume, mm^3	7.75 ± 0.41	7.51 ± 0.37	0.012
SRF configurations			
Volume, mm^3	0.93 ± 0.94	0.67 ± 0.53	0.184
PH, μm	298.13 ± 92.67	192.97 ± 71.05	<0.001
GBD, μm	3259.23 ± 997.17	3385.80 ± 1264.63	0.643
Area, mm^2	8.29 ± 5.22	9.00 ± 5.31	0.583
PH/GBD ratio, %	9.44 ± 2.57	5.97 ± 1.90	<0.001
Vertical eccentricity, %	7.10 ± 5.02	15.80 ± 13.66	0.002
Type of basal area, a:b	29:10	14:16	0.019†
PED configurations			
N of eyes, %	37, 94.9%	28, 93.3%	1.000‡
Volume, mm^3	0.04 ± 0.07	0.01 ± 0.02	0.063
PH, μm	99.68 ± 100.55	53.68 ± 23.00	0.010
GBD, μm	725.97 ± 291.10	935.18 ± 499.01	0.055
Area, mm^2	0.33 ± 0.37	0.30 ± 0.28	0.716
PH/GBD ratio, %	13.89 ± 10.44	8.02 ± 6.78	0.008

CMT, central subfield thickness; CPT, central point thickness; MV, total macular volume. SRF type of basal area: a, circular or horizontal; b, vertical.

* *t*-test for continuous variables.

† χ^2 test for categorical variables.

‡ Fisher's exact test for categorical variables. Continuous variables are expressed as mean ± SD.

parameter when diagnosing chronic CSC at an initial visit for patients with an unclear date of symptom onset.

A number of studies have evaluated the periodic changes in CSC,[14,28–35] and FA analysis studies have provided some insights about the natural course of CSC.[29–33] With the introduction of OCT, studies of the CSC have focused on the change of microstructures in the retina and choroid.[14,34,35] In the current study, we focused on the morphology of SRF and showed early periodic changes of 3D configurations in CSC beyond two-dimensional tomographic morphology. The analysis of early periodic changes demonstrated that acute CSC showed a significantly greater amount of change related to the volume, PH, GBD, and basal area of SRF compared to chronic CSC. In acute CSC, dynamic changes were observed during the early period and the changing pattern was different depending on the presence of SRF at 3 months. The majority of patients in the spontaneously resolving group showed in situ decrease or symmetric shrinking of the lesion. However, in the persistent

Table 3. Early Periodic Changes in 3D Configurations of CSC

	Acute CSC, $n = 31$	Chronic CSC, $n = 21$	*P* Value*
Age, y	44.48 ± 7.72	47.62 ± 7.97	0.162
Sex, M:F	21:10	16:5	0.509†
Recurrence history, first:recurrent	20:11	9:12	0.123†
OCT interval, days	35.19 ± 6.20	32.52 ± 3.56	0.081
ΔCMT, μm	31.11 ± 33.33	10.86 ± 10.50	0.002
ΔCPT, μm	165.10 ± 123.83	44.14 ± 40.69	<0.001
ΔMV, mm^3	0.87 ± 0.94	0.20 ± 0.18	0.001
ΔPRL volume, mm^3	0.21 ± 0.16	0.11 ± 0.08	0.006
SRF configurations			
Δ volume, mm^3	0.68 ± 0.83	0.20 ± 0.26	0.004
Δ volume, %	57.01 ± 26.84	24.58 ± 19.55	<0.001
Δ PH, μm	162.35 ± 115.06	45.90 ± 51.96	<0.001
Δ GBD, μm	1271.42 ± 1155.50	548.71 ± 562.61	0.004
Δ area, mm^2	4.59 ± 4.20	2.11 ± 2.29	0.008
Δ PH/GBD ratio, %	4.48 ± 3.52	1.56 ± 1.63	<0.001
PED configurations			
Δ volume, mm^3	0.02 ± 0.03	0.00 ± 0.01	0.013
Δ PH, μm	40.48 ± 55.39	16.62 ± 14.34	0.028
Δ GBD, μm	279.87 ± 281.65	179.43 ± 149.14	0.102
Δ area, mm^2	0.14 ± 0.15	0.07 ± 0.12	0.077
Δ PH/GBD ratio, %	7.63 ± 8.28	3.01 ± 4.91	0.015

* *t*-test for continuous variables.

† χ^2 test for categorical variables. Continuous variables are expressed as mean ± SD.

Table 4. Correlation Between the Change of SRF Volume and Those of Other Parameters in Acute and Chronic CSC

	Acute CSC, $n = 31$		Chronic CSC, $n = 21$	
	rho	*P* Value*	*rho*	*P* Value*
Δ SRF volume vs. Δ PRL volume	0.363	0.045	0.238	0.299
vs. Δ PED volume	0.153	0.411	−0.034	0.883
vs. Δ PH	0.545	0.002	0.357	0.113
vs. Δ GBD	0.406	0.023	0.181	0.433
vs. Δ area	0.677	<0.001	0.165	0.475

* Spearman's correlation.

group, the SRF moved and elongated due to the effect of gravity in more than half of the patients. In chronic CSC, vertical eccentricity of SRF was greater than in the acute group and the percentage of basal area with vertical oval type was larger than that with circular or horizontal oval type. These results suggested that the vertical eccentricity and the type of basal area of SRF might be the parameters that can be used to determine the chronicity of CSC. The changing pattern of 3D configurations could be useful for predicting the course of CSC. However, additional studies with larger cohorts are mandatory to verify the possibility of clinical application of this study.

In a previous FA study, Yannuzzi et al. reported that there were some cases of chronic CSC with inferior gravitational tracts that extended from the macula or disc to well below the inferior arcades, which often was described as an hourglass configuration.[36] Previous investigators presumed that the gravitational tracts were produced by SRF due to a high specific gravity, and sank toward the inferior fundus and dissected through the subretinal space.[28,36] OCT is a noninvasive method that can be used to measure the change of the configuration. However, very few studies did time- and gravity-related observations using SDOCT. Our study sought to visualize the effect of the force of gravity on the shape of SRF using newly derived OCT parameters. These parameters reflected the extent of inferior shifting that was a result of the gravitational effect on SRF. Because the effect of gravity becomes greater with the persistence of SRF, OCT parameters reflecting the gravitational effect on SRF could be higher depending on the duration of SRF before initial visit.

SDOCT provides highly resolved images and permits identification of microstructural changes, as well as a 3D view of the macular configuration. Furthermore, the advanced built-in software program of SDOCT provides easy and reliable measurements. Our study used the SDOCT technology to generate OCT images that allowed investigation and analysis of 3D configurations of SRF and PED in eyes with different stages of CSC. Although it needs manual

Table 5. Comparison Between Spontaneously Resolving and Persistent Types

	Spontaneously Resolving Type, $n = 17$	Persistent Type, $n = 12$	*P* Value*
Age, y	43.47 ± 6.35	47.25 ± 4.50	0.088
Sex, M:F	11:6	8:4	1.000†
Symptom duration, d	27.59 ± 23.91	26.42 ± 21.86	0.835
Recurrence history, first:recurrent	12:5	7:5	0.694†
OCT interval, d	35.94 ± 6.35	33.92 ± 6.56	0.411
CMT, μm‡	291.7 (286.5, 321.4)	298.2 (290.8, 309.7)	0.499
MV, mm^3‡	8.25 (8.11, 9.09)	8.51 (8.27, 8.76)	0.419
PRL volume, mm^3‡	7.75 (7.56, 7.99)	7.91 (7.50, 8.04)	0.811
SRF at the initial visit			
Volume, mm^3‡	0.53 (0.39, 0.98)	0.65 (0.41, 1.50)	0.845
PH, μm‡	272.0 (219.5, 357.0)	306.5 (258.3, 395.0)	0.556
GBD, μm‡	3362.0 (2663.0, 3767.0)	3285.5 (2466.3, 4230.0)	0.983
Area, mm^2‡	7.73 (5.20, 9.21)	8.14 (4.24, 12.34)	0.983
PH/GBD ratio, %‡	8.00 (7.25, 10.15)	10.10 (8.13, 10.63)	0.245
Vertical eccentricity, %‡	7.80 (4.70, 13.25)	5.35 (3.18, 13.53)	0.303
Type of basal area, a:b	13:4	8:4	0.683†
Periodic changes of SRF			
Δ volume, mm^3‡	0.52 (0.32, 0.81)	0.30 (0.07, 0.52)	0.043
Δ volume, %‡	76.92 (69.13, 84.52)	27.09 (17.26, 40.65)	<0.001
Δ PH, μm‡	204.0 (101.0, 279.5)	62.0 (38.3, 151.0)	0.012
Δ GBD, μm‡	1511.0 (482.0, 2771.0)	228.5 (147.8, 392.8)	0.005
Δ area, mm^2‡	4.15 (2.63, 7.71)	1.06 (0.42, 2.93)	0.002
Δ PH/GBD ratio, %‡	5.10 (2.00, 7.90)	2.55 (1.40, 5.15)	0.245
Basal area expansion, eyes	0 (0.0%)	6 (50.0%)	0.002†
Changing pattern of SRF, a:b	16:1	5:7	0.003†

Type of basal area: a, circular or horizontal; b, vertical. Changing pattern of SRF: a, in situ decrease; b, downward elongated type.
* *t*-test or Mann-Whitney *U* test for continuous variables;
† Fisher's exact test for categorical variables.
‡ Continuous variables are expressed as median (interquartile range).

modification of segmentation lines to generate 3D images of SRF, the measurement of the 3D configurations would be useful to manage patients with CSC.

Our study was limited by small sample size of each group and by the retrospective design. Although 120 participants were reviewed, only 69 were eligible for the study. The results of our study could not represent all the patients in the clinics. However, we had intended to exclude cases with possible compounding factors that might have influenced the change of SRF in idiopathic CSC. The CSC stage was determined based on the onset of subjective symptoms stated by the patient, which may differ from the exact onset of symptoms. While we focused on the change of SRF, we did not compare the characteristics of microstructure, such as photoreceptor inner/outer segments between groups. Another limitation of this study is inclusion of some cases with a large SRF area extending beyond the 6×6 mm cube scan boundary. In these cases, the area was determined on the fundus photography obtained with the OCT. Because of these limitations, there may be some errors in the measurement values. However, only six relevant cases had this limitation, and there were no cases where the image area exceeded more than 10% of the total area.

In conclusion, 3D configurations of SRF were different between acute and chronic CSC. Chronic CSC showed less dynamic changes of SRF. Our study suggested that, in patients with acute CSC, the changing pattern of 3D configurations during the first month could be different according to the persistence of SRF.

Acknowledgments

Presented in part at the 12th EURETINA Congress, Milan, Italy, September 6–9, 2012.

Supported by a grant from the Korean Health Technology R&D Project, Ministry for Health, Welfare & Family Affairs, Republic of Korea (A102024).

Disclosure: **S.-E. Ahn**, None; **J. Oh**, None; **J.-H. Oh**, None; **I.K. Oh**, None; **S.-W. Kim**, None; **K. Huh**, None

References

1. Spaide RF, Campeas L, Haas A, et al. Central serous chorioretinopathy in younger and older adults. *Ophthalmology*. 1996;103:2070–2079.
2. Gemenetzi M, De Salvo G, Lotery AJ. Central serous chorioretinopathy: an update on pathogenesis and treatment. *Eye (Lond)*. 2010;24:1743–1756.
3. Hee MR, Puliafito CA, Wong C, et al. Optical coherence tomography of central serous chorioretinopathy. *Am J Ophthalmol*. 1995;120:65–74.
4. Ojima Y, Hangai M, Sasahara M, et al. Three-dimensional imaging of the foveal photoreceptor layer in central serous chorioretinopathy using high-speed optical coherence tomography. *Ophthalmology*. 2007;114:2197–2207.
5. Kamppeter B, Jonas JB. Central serous chorioretinopathy imaged by optical coherence tomography. *Arch Ophthalmol*. 2003;121:742–743.
6. Montero JA, Ruiz-Moreno JM. Optical coherence tomography characterization of idiopathic central serous chorioretinopathy. *Br J Ophthalmol*. 2005;89:562–564.
7. van Velthoven ME, Verbraak FD, Garcia PM, et al. Evaluation of central serous retinopathy with en face optical coherence tomography. *Br J Ophthalmol*. 2005;89:1483–1488.
8. Saito M, Iida T, Kishi S. Ring-shaped subretinal fibrinous exudate in central serous chorioretinopathy. *Jpn J Ophthalmol*. 2005;49:516–519.
9. Piccolino FC, de la Longrais RR, Ravera G, et al. The foveal photoreceptor layer and visual acuity loss in central serous chorioretinopathy. *Am J Ophthalmol*. 2005;139:87–99.
10. Mitarai K, Gomi F, Tano Y. Three-dimensional optical coherence tomographic findings in central serous chorioretinopathy. *Graefes Arch Clin Exp Ophthalmol*. 2006;244:1415–1420.
11. Hussain N, Baskar A, Ram LM, Das T. Optical coherence tomographic pattern of fluorescein angiographic leakage site in acute central serous chorioretinopathy. *Clin Experiment Ophthalmol*. 2006;34:137–140.
12. Hirami Y, Tsujikawa A, Sasahara M, et al. Alterations of retinal pigment epithelium in central serous chorioretinopathy. *Clin Experiment Ophthalmol*. 2007;35:225–230.
13. Shukla D, Aiello LP, Kolluru C, et al. Relation of optical coherence tomography and unusual angiographic leakage patterns in central serous chorioretinopathy. *Eye*. 2008;22:592–596.
14. Iida T, Hagimura N, Sato T, Kishi S. Evaluation of central serous chorioretinopathy with optical coherence tomography. *Am J Ophthalmol*. 2000;129:16–20.
15. Wang GH, Zhang J, Zhang D, Lv FL, Wang LX. Value of three-dimensional optical coherence tomography and fundus photochromy in correlating the fluorescein leaking sites of acute central serous chorioretinopathy. *Med Princ Pract*. 2011;20:283–286.
16. Kim SW, Oh J, Kwon SS, Yoo J, Huh K. Comparison of choroidal thickness among patients with healthy eyes, early age-related maculopathy, neovascular age-related macular degeneration, central serous chorioretinopathy, and polypoidal choroidal vasculopathy. *Retina*. 2011;31:1904–1911.
17. Kim SW, Oh J, Huh K. Correlations among various functional and morphological tests in resolved central serous chorioretinopathy. *Br J Ophthalmol*. 2012;96:350–355.
18. Song IS, Shin YU, Lee BR. Time-periodic characteristics in the morphology of idiopathic central serous chorioretinopathy evaluated by volume scan using spectral-domain optical coherence tomography. *Am J Ophthalmol*. 2012;154:366–375.
19. Liew G, Quin G, Gillies M, Fraser-Bell S. Central serous chorioretinopathy: a review of epidemiology and pathophysiology. *Clin Experiment Ophthalmol*. 2013;41:201–214.
20. Drexler W, Fujimoto JG. State-of-the-art retinal optical coherence tomography. *Prog Retin Eye Res*. 2008;27:45–88.
21. Benson SE, Schlottmann PG, Bunce C, et al. Assessment of the reproducibility and repeatability of a method of grading macular subretinal fluid using optical coherence tomography. *Eye*. 2006;20:1030–1033.
22. Nakajima H, Mizota A, Tanaka M. Technical note: method for estimating volume of subretinal fluid in cases of localized retinal detachment by OCT ophthalmoscopy. *Ophthalmic Physiol Opt*. 2007;27:512–517.
23. Heussen FM, Ouyang Y, Sadda SR, Walsh AC. Simple estimation of clinically relevant lesion volumes using spectral domain-optical coherence tomography in neovascular age-related macular degeneration. *Invest Ophthalmol Vis Sci*. 2011;52:7792–7798.
24. Shin JW, Shin YU, Lee BR. Choroidal thickness and volume mapping by a six radial scan protocol on spectral-domain optical coherence tomography. *Ophthalmology*. 2012;119:1017–1023.
25. Ross A, Ross AH, Mohamed Q. Review and update of central serous chorioretinopathy. *Curr Opin Ophthalmol*. 2011;22:166–173.
26. Fujimoto H, Gomi F, Wakabayashi T, Sawa M, Tsujikawa M, Tano Y. Morphologic changes in acute central serous chorioretinopathy evaluated by Fourier-domain optical coherence tomography. *Ophthalmology*. 2008;115:1494–1500.

27. Shinojima A, Hirose T, Mori R, Kawamura A, Yuzawa M. Morphologic findings in acute central serous chorioretinopathy using spectral domain-optical coherence tomography with simultaneous angiography. *Retina*. 2010;30:193–202.
28. Wang M, Munch IC, Hasler PW, Prünte C, Larsen M. Central serous chorioretinopathy. *Acta Ophthalmol*. 2008;86:126–145.
29. Gilbert CM, Owens SL, Smith PD, Fine SL. Long-term follow-up of central serous chorioretinopathy. *Br J Ophthalmol*. 1984; 68:815–820.
30. Castro-Correia J, Coutinho MF, Rosas V, Maia J. Long-term follow-up of central serous retinopathy in 150 patients. *Doc Ophthalmol*. 1992;81:379–386.
31. Ciardella AP, Guyer DR, Spitznas M, et al. Central serous chorioretinopathy. In: Ryan SJ, ed. *Retina*. 3rd ed. Vol. 2. St. Louis, MO: The C. V. Mosby Co. 2001:1153–1181.
32. Bujarborua D. Long-term follow-up of idiopathic central serous chorioretinopathy without laser. *Acta Ophthalmol Scand*. 2001;79:417–421.
33. Loo RH, Scott IU, Flynn HW Jr, et al. Factors associated with reduced visual acuity during long-term follow-up of patients with idiopathic central serous chorioretinopathy. *Retina*. 2002;22:19–24.
34. Wang MS, Sander B, Larsen M. Retinal atrophy in idiopathic central serous chorioretinopathy. *Am J Ophthalmol*. 2002; 133:787–793.
35. Hata M, Oishi A, Shimozono M et al. Early changes in foveal thickness in eyes with central serous chorioretinopathy. *Retina*. 2013;33:296–301.
36. Yannuzzi LA, Shakin JL, Fisher YL, Altomonte MA. Peripheral retinal detachments and retinal pigment epithelial atrophic tracts secondary to central serous pigment epitheliopathy. *Ophthalmology*. 1984;91:1554–1572.

Investigative Ophthalmology & Visual Science